ADVANCED FUNCTIONAL MATERIALS
www.afm-journal.de

Configurational Isomers Induced Significant Difference in All-Polymer Solar Cells

*Hengtao Wang, Hui Chen, Weicheng Xie, Hanjian Lai, Tingxing Zhao, Yulin Zhu, Lin Chen, Chunxian Ke, Nan Zheng, and Feng He**

The design of polymer acceptors plays an essential role in the performance of all-polymer solar cells. Recently, the strategy of polymerized small molecules has achieved great success, but most polymers are synthesized from the mixed monomers, which seriously affects batch-to-batch reproducibility. Here, a method to separate γ-Br-IC or δ-Br-IC in gram scale and apply the strategy of monomer configurational control in which two isomeric polymeric acceptors (PBTIC-γ-2F2T and PBTIC-δ-2F2T) are produced is reported. As a comparison, PBTIC-*m*-2F2T from the mixed monomers is also synthesized. The γ-position based polymer (PBTIC-γ-2F2T) shows good solubility and achieves the best power conversion efficiency of 14.34% with a high open-circuit voltage of 0.95 V when blended with PM6, which is among the highest values recorded to date, while the δ-position based isomer (PBTIC-δ-2F2T) is insoluble and cannot be processed after parallel polymerization. The mixed-isomers based polymer, PBTIC-*m*-2F2T, shows better processing capability but has a low efficiency of 3.26%. Further investigation shows that precise control of configuration helps to improve the regularity of the polymer chain and reduce the π–π stacking distance. These results demonstrate that the configurational control affords a promising strategy to achieve high-performance polymer acceptors.

1. Introduction

Benefitting from the efforts and remarkable works of many scientists, all-polymer solar cells (all-PSC) have made great progress over the last 25 years.[1–5] Recently, the power conversion efficiencies (PCEs) of all-PSCs have been improved to 14–15%. A major contributor to this improvement was the incorporation of the acceptor–(donor–acceptor–donor)–acceptor (A–DAD–A) electron-deficient type polymerization unit in the polymer acceptor.[6–10]

In order to enrich the polymer acceptors for all-PSCs, many strategies have been proposed and many polymers have been synthesized. An important milestone was the application of donor–acceptor (D–A) polymerization in 2007[11] following which, several polymer acceptors based on naphthalene diimide (NDI)[12–14] or perylenediimide (PDI)[15,16] were synthesized. The most representative of those polymer acceptors was N2200, which is widely used in organic solar cells (OSC).[17] Other A-type units, such as isoindigo,[18] B→N bridged bipyridine,[19] and cyanobenzothiadiazole[20] were also applied and contributed significantly to the forward progress of all-PSCs. In 2017, Zhang et al. proposed a strategy of polymerizing small molecular acceptors (PSMA) with an appropriate proper linker and obtained PZ1, a high-performance polymeric acceptor.[21] Devices based on PZ1 at that time achieved a PCE of 9.19%. It should be mentioned that polymers based on this strategy will have the properties of both SMAs and polymer acceptors. Accordingly, a series of PSMAs based on IDIC,[22–26] ITIC,[27–29] and BTIC[5–9,30,31] were synthesized, and a remarkable advance in all-polymer solar cells was achieved.

Although great progress has been made in recent years, it should be noted that most of the high-performance n-type polymers are synthesized from mixtures of two monomers with γ-Br-IC or δ-Br-IC end functional groups. The monomers of these n-type polymers are a mixture of three components, and this negatively affects the batch-to-batch reproducibility. Furthermore, the randomly distributed units in the polymer discourage the molecular planarity which affects intermolecular packing and decreases the charge transfer. Our previous work also confirmed that the isomerism of the bromine end groups led to

Dr. H. Wang, Dr. H. Chen, W. Xie, H. Lai, Dr. T. Zhao, Y. Zhu, L. Chen, C. Ke, Prof. F. He
Shenzhen Grubbs Institute and Department of Chemistry
Southern University of Science and Technology
Shenzhen 518055, China
E-mail: hef@sustech.edu.cn

Dr. H. Chen
Academy for Advanced Interdisciplinary Studies
Southern University of Science and Technology
Shenzhen 518055, China

Dr. N. Zheng
Institute of Polymer Optoelectronic Materials and Devices
State Key Laboratory of Luminescent Materials and Devices
South China University of Technology
Guangzhou 510640, China

Prof. F. He
Guangdong Provincial Key Laboratory of Catalysis
Southern University of Science and Technology
Shenzhen, Guangdong 518055, China

The ORCID identification number(s) for the author(s) of this article can be found under https://doi.org/10.1002/adfm.202100877.

DOI: 10.1002/adfm.202100877

notable structural differences in small-molecular non-fullerene acceptors.[32,33] Recently, Yang and coworker utilized thiophene as linker and synthesized two configuration-confirmed polymer acceptors, PY-IT and PY-OT. The following tests showed that PY-IT significantly improved the fill factor (FF) in the devices and delivered an extremely high performance in all-polymer organic solar cells.[34] Hence, the development of configurationally defined polymer would be a promising strategy to understand the anomeric effect in all-polymer solar cells and lead to the high performance n-type polymer acceptors. Apparently, the isolation of γ-Br-IC and δ-Br-IC was the key factor to obtain the pure monomers for the further polymerization. Recrystallization from chloroform and ethanol proved to be an effective way to separate the Cl-substituted isomers,[35] but it is not very efficient to separate Br-substituted isomers, especially to obtain the δ-Br-IC isomer. From this point, it is very necessary to find out a more effective way to collect the γ-Br-IC and δ-Br-IC in large scale, such as in gram scale. Based on that, the researchers in this field can have the capability to make a deep insight of the isomeric effect in the all-polymer solar cells. What's more important, a deep exploration of the polymerization of these isomer-free units and other conjugated linking moieties could deliver better understanding of the configurational control in polymer solar cell, and further pump the performance blooming in this area.

Herein, we applied the strategy of configurational control in the design of acceptors with isolated γ-Br-IC and δ-Br-IC at large scale, and successfully produced the two polymers, PBTIC-γ-2F2T and PBTIC-δ-2F2T, shown in **Scheme 1**. In the formation of these polymers, fluorinated 2,2′-bithiophene was used as the linker in the polymerization in an effort to tune the energy gap[36–38] and enhance the intermolecular non-covalent interactions[39,40] of the final polymeric acceptors. In order to gain deeper insight in this system, we also used the mixed monomers *m*-Br-BTIC in the polymerization and thus achieved the polymer acceptor PBTIC-*m*-2F2T as a comparison. Interestingly, those three polymers PBTIC-γ-2F2T, PBTIC-δ-2F2T, and PBTIC-*m*-2F2T have significantly different physicochemical properties. PBTIC-γ-2F2T dissolves easily in common solvents such as dichloromethane (DCM), chloroform (CF), and chlorobenzene (CB). In contrast, PBTIC-δ-2F2T shows very poor solubility in these solvents, and it results in almost opposite photovoltaic properties in their devices. PBTIC-γ-2F2T shows the best photovoltaic performance among these materials and achieves a PCE of 14.34% with a high V_{oc} of 0.95 V. It was very hard to process PBTIC-δ-2F2T in solution due to its poor solubility, which resulted in almost zero efficiency in devices, and hindered the further investigation of the polymer's photovoltaic properties. The bad solubility of PBTIC-δ-2F2T mainly results from the strong aggregation because of the "V"-type polymer chain in PBTIC-δ-2F2T, and leads to smaller intramolecular hindrance and higher planarity. PBTIC-*m*-2F2T showed modest solubility but the photovoltaic performance is only about 3.26% in efficiency, much lower than that of PBTIC-γ-2F2T. The diminished efficiency is mainly caused by the electron mobility which is almost 2 orders of magnitude lower than that of PBTIC-γ-2F2T. In order to further explore the isomerism effect in this system, 2,2-bithiophene was also incorporated as a linker to deliver PBTIC-γ-2T, a non-fluorinated polymer. Unsurprisingly,

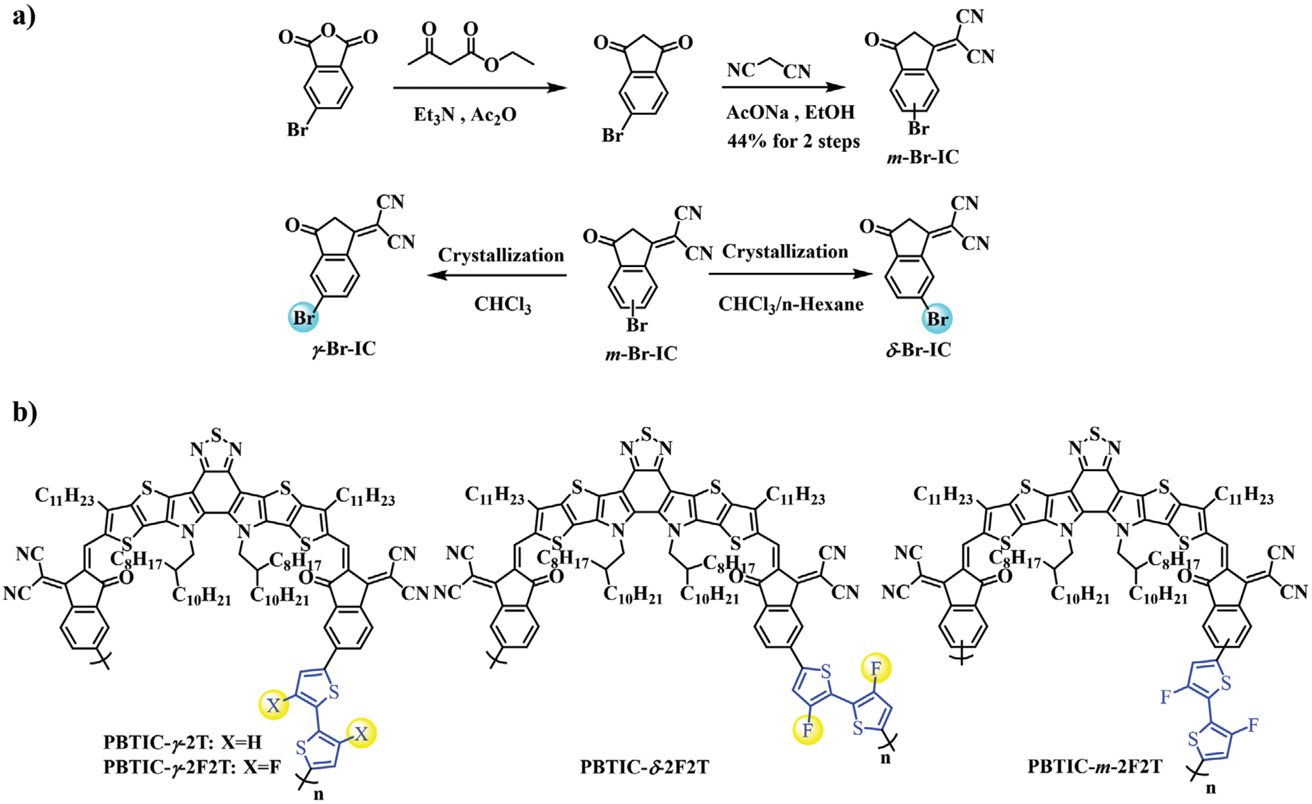

Scheme 1. a) Synthetic route to *m*-Br-IC, γ-Br-IC, and δ-Br-IC; b) Structures of PBTIC-γ-2F2T, PBTIC-δ-2F2T, PBTIC-*m*-2F2T, and PBTIC-γ-2T.

this polymer also showed good performance with a PCE of 11.92%. The performance of PBTIC-γ2T, which is slightly lower than that of PBTIC-γ2F2T is mainly due to the decreased planarity and charge mobility in these polymer acceptors. Hence, configurational control of monomers offers an opportunity to enhance the charge mobility in polymer acceptors and eventually elevate the device performance of all-polymer solar cells.

2. Results and Discussion

2.1. Materials Design and Synthesis

The synthesis of the three end caps, m-Br-IC, γ-Br-IC, and δ-Br-IC is shown in Scheme 1. m-Br-IC was produced in two steps from 4-bromoisobenzofuran-1,3-dione. γ-Br-IC was crystallized from CF with minor modifications of our reported method.[33] δ-Br-IC was obtained by crystallization from the CF/hexane. It deserved to mention that both brominated isomers could be obtained in gram scales, which brought great convenience for the further investigation of the isomeric effect in the OSCs. Detailed information can be found in Supporting Information (SI), in which Scheme S1 describes the synthetic route to the polymer acceptors, PBTIC-γ2F2T, PBTIC-δ2F2T, PBTIC-m-2F2T, and PBTIC-γ2T. The three end caps were connected with BT-CHO through a Knoevenagel condensation to achieve the corresponding monomers, γ-Br-BTIC, δ-Br-BTIC, and m-Br-BTIC, and the monomers obtained in this way underwent Pd catalyzed polymerization with 5,5′-bis(trimethylstannyl)-3,3′-difluoro-2,2′-bithiophene and 5,5′-bis(trimethylstannyl)-2,2′-bithiophene to afford the target polymer acceptors. PBTIC-γ2F2T, PBTIC-*m*-2F2T, and PBTIC-γ2T exhibit good solubility in CF and CB, but PBTIC-δ2F2T with really strong aggregation showed insolubility in these solvents. The reaction times were adjusted to lower the molecular weight of the polymeric product, but the PBTIC-δ2F2T that was produced still exhibited strong aggregation which hindered further investigation of its properties. Thermogravimetric analysis (TGA) showed that all of these polymers exhibit good thermal stability with 5% weight-loss at temperatures above 340 °C as shown in Figure S1, Supporting Information, and the results are summarized in Table S1, Supporting Information. PBTIC-γ2F2T showed the highest stability and achieved a 5% weight-loss temperature of 362 °C. Differential scanning calorimetry (DSC) showed that all these materials have high morphological stability. No obvious melting temperature and crystallization temperature were observed when the materials were heated up to 250 °C or cooled down to 30 °C (Figure S2, Supporting Information), which means a stable state in the blend films and this is very important for the morphological stability in the devices.

2.2. Physicochemical Properties

The optical properties of PBTIC-γ2F2T, PBTIC-*m*-2F2T, and PBTIC-γ2T were assessed both in solution and as thin films, and are shown in **Figure 1**a with the parameters summarized in **Table 1**. We also attempted to measure the UV–vis absorption

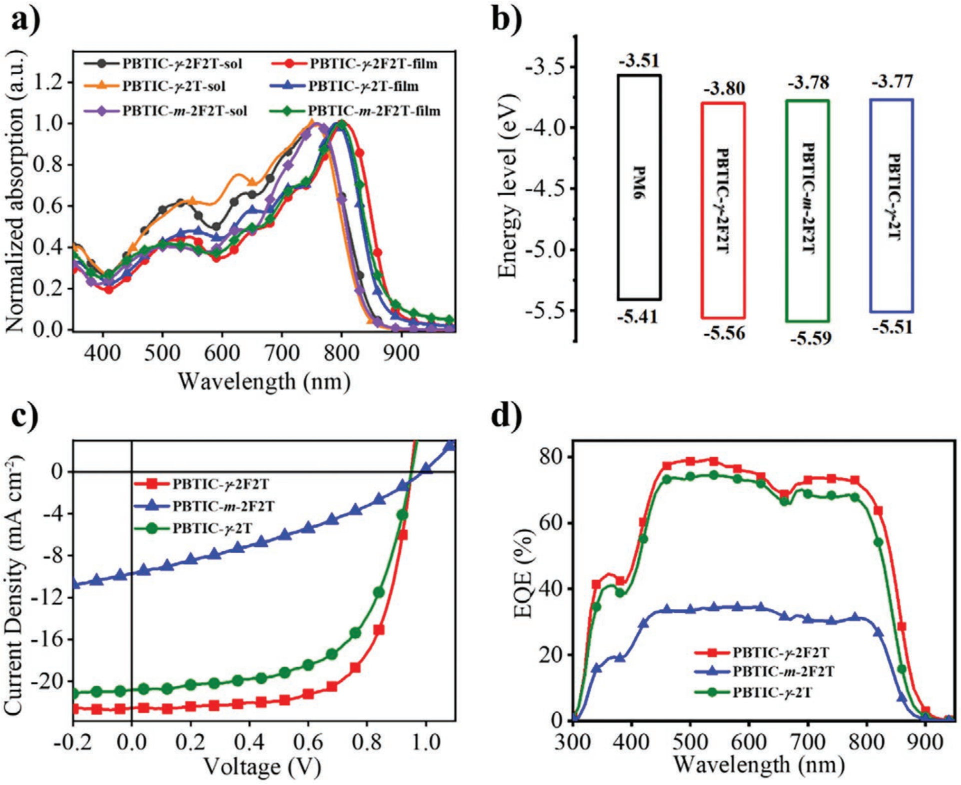

Figure 1. a) Normalized absorption spectra of PBTIC-γ2F2T, PBTIC-*m*-2F2T, and PBTIC-γ2T in CF solution and in thin films. b) Energy level diagrams of PM6, BTIC-γ2F2T, PBTIC-*m*-2F2T, and PBTIC-γ2T series. c) *J-V* characteristics of device based on PBTIC-γ2F2T, PBTIC-*m*-2F2T, and PBTIC-γ2T. d) EQE spectra of PBTIC-γ2F2T, PBTIC-*m*-2F2T, and PBTIC-γ2T based devices.

Table 1. UV–vis absorption, and electrochemical properties of PBTIC-γ2F2T, PBTIC-*m*-2F2T, and PBTIC-γ2T.

Acceptors	λ_{max}^{sol} [nm]	λ_{max}^{film} [nm]	λ_{onset}^{film} [nm]	$E_g^{opt\,a)}$ [eV]	$E_{HOMO}^{b)}$ [eV]	$E_{LUMO}^{c)}$ [eV]
PBTIC-γ2F2T	758	805	882	1.41	−5.56	−3.80
PBTIC-*m*-2F2T	758	790	866	1.43	−5.59	−3.78
PBTIC-γ2T	759	796	871	1.42	−5.51	−3.77
PBTIC-δ2F2T	747	802	895	1.39	−5.58	−3.83

a) $E_g^{opt} = 1240/\lambda_{onset}$; b) $E_{LUMO} = -(E_{red} + 4.46)$; c) $E_{HOMO} = -(E_{ox} + 4.46)$.

spectrum of PBTIC-δ2F2T and details can be found in Figures S5 and S6, Supporting Information. The parameters were also summarized in Table 1. PBTIC-γ2F2T, PBTIC-*m*-2F2T, and PBTIC-γ2T showed similar absorption in the 500–800 nm range and similar maximum absorption peaks at ≈758 nm in solution, while PBTIC-δ2F2T at 747 nm. The apparent different absorption peaks of PBTIC-γ2F2T and PBTIC-δ2F2T might be caused by the side effects of substitution on electronic properties of the backbone. PBTIC-γ2F2T shows stronger absorption with an absorption coefficient of over 1.24×10^5 M^{-1} cm^{-1} (Figure S3, Supporting Information) compared with PBTIC-*m*-2F2T (1.15×10^5 M^{-1} cm^{-1}) and PBTIC-γ2T (1.02×10^5 M^{-1} cm^{-1}). This is attributed to the fluorination and the regular arrangement along the polymer chain. In the thin film, the absorption peaks of PBTIC-γ2F2T and PBTIC-δ2F2T red shifted to 805 and 802 nm which were 15 nm and 12 nm higher than that of PBTIC-*m*-2F2T, respectively. This proved that precise control of configuration could enhance the intermolecular packing and broaden the absorption spectra, benefitting the J_{sc} in the devices. It was interesting to find that the non-fluorinated polymer, PBTIC-γ2T also exhibited 6 nm redshift in the film when compared to PBTIC-*m*-2F2T, which again demonstrates that precise control of the molecular structure can enhance the intermolecular π–π stacking and thus benefit the intermolecular charge transportation.

Cyclic voltammetry (CV) was used to determine the energy levels of the polymer acceptors, and the results are shown in Figure 1b, and Figures S4 and S5, Supporting Information. A ferrocene–ferrocenium (Fc/Fc$^+$) redox couple was chosen as the calibrating potential, and the onset oxidation/reduction potentials versus Ag/Ag$^+$ were 1.10/–0.66 eV for PBTIC-γ2F2T, 1.12/–0.63 eV for PBTIC-δ2F2T, 1.13/–0.68 eV for PBTIC-*m*-2F2T, and 1.05/–0.69 eV for PBTIC-γ2T. Hence, the HOMO/LUMO energy levels of PBTIC-γ2F2T, PBTIC-δ2F2T, PBTIC-*m*-2F2T, and PBTIC-γ2T were –5.56/–3.80, –5.58/–3.83, –5.59/–3.78, and –5.51/–3.77 eV, respectively, and the corresponding results are summarized in Table 1. The LUMO energy levels of PBTIC-γ2F2T and PBTIC-δ2F2T were lower than the other two, and this will enhance the exciton dissociation at the interlayer of the donor and acceptor. The bandgap of PBTIC-γ2F2T and PBTIC-δ2F2T were smaller than that of PBTIC-*m*-2F2T, which might imply a better intermolecular packing and higher charge transport in devices based on these polymers.

In order to investigate the configuration of these molecules and the distribution of the electronic atmosphere, density functional theory (DFT) was employed with B3LYP/6-31G (d,p), in which the undecyl and octyldodecyl chains were simplified and represented as methyl and isobutyl groups. Since PBTIC-*m*-2F2T was randomly polymerized from the mixed isomers *m*-Br-BTIC, theoretic calculations were not performed. As shown in Figure S8, the fluorinated molecule, PBTIC-γ2F2T, showed higher planarity than the non-fluorinated polymer, PBTIC-γ2T. It was found that introduction of a fluorine atom into the bithiophene unit decreased the dihedral angle between the two thiophene units from 15.41° to 0.34°, significantly improving the planarity of PBTIC-γ2F2T. This was attributed to the intramolecular F-S interaction, the measured F···S distance being 2.94 Å. The improved molecular planarity might result from a smaller steric hindrance when attached to the BTIC unit and could improve the intermolecular packing and charge mobility, which will benefit the photovoltaic performance. Polymerization at different sites also affected the molecular configuration as the δ-position based polymer, PBTIC-δ2F2T, showed higher flexibility with a "V"-shaped backbone. This special configuration could be expected to improve the intermolecular π–π stacking between BTIC units and enhance the intermolecular electron transport. However, the resulting strong aggregation would significantly lower the solubility and make PBTIC-δ2F2T difficult to process in solution. Figure S9, Supporting Information, shows the calculated HOMO and LUMO energy levels and the electron distribution across the molecular backbones of PBTIC-γ2F2T, PBTIC-δ2F2T, and PBTIC-γ2T. It was found that all three of these polymers hold the same calculated HOMO energy levels of –5.43 eV, and the calculated LUMO of PBTIC-γ2F2T (–3.39 eV) and PBTIC-δ2F2T (–3.39 eV) were slightly deeper than that of PBTIC-γ2T (–3.38 eV), which is consistent with the cyclic voltammetry data.

2.3. Photovoltaic Performance

In order to explore the photovoltaic performance, devices based on these materials with the structure of ITO/TEDOT:PSS/PM6:acceptor/PNDIT-F3N/Ag were fabricated. The current density versus voltage (*J–V*) curves are shown in Figure 1c, and the corresponding parameters are summarized in **Table 2**. The device based on PBTIC-γ2F2T showed the highest PCE of 14.34% with a current density (J_{sc}) of 22.56 mA cm^{-2} and fill factor (*FF*) of 66.89%, which is much higher than that of PBTIC-*m*-2F2T whose PCE is 3.26%. Apparently, the improved efficiency of PBTIC-γ2F2T mainly comes from the improved J_{sc} and *FF*, which in turn is attributed to the red-shifted absorption and higher charge mobility. However, the process of PBTIC-δ2F2T proved to be really difficult due to the terrible solubility, and the resulted blend film seemed to be apparently different from others. Not surprisingly, the corresponding device exhibited almost zero efficiency (0.02%) under the test conditions (Table 2). The device based on the non-fluorinated polymer, PBTIC-γ2T, also exhibited good performance with a PCE of

Table 2. Photovoltaic parameters of the polymer acceptor based OSC devices.

Donor: Acceptor[a)]	V_{oc} [V]	J_{sc} [mA cm^{-2}]	FF [%]	PCE [%]
PM6: PBTIC-*γ*-2F2T	0.95	22.56	66.89	14.34
PM6: PBTIC-*m*-2F2T	0.99	9.72	33.84	3.26
PM6: PBTIC-*δ*-2F2T	0.08	0.91	24.83	0.02
PM6: PBTIC-*γ*-2T	0.95	20.85	60.22	11.92

[a)] 1-chloronaphthalene (CN) (volume ratio: 0.5%) was added into solutions as additives.

11.92% (V_{oc} = 0.95, J_{sc} = 20.85 mA cm^{-2}, FF = 60.22%). Hence, the strategy of precise configurational control appears to be an effective strategy to improve the performance of all-PSCs.

The external quantum efficiency (EQE) of these polymer acceptors based on all-PSCs are shown in Figure 1d. It was found that both PBTIC-*γ*-2F2T and PBTIC-*γ*-2T based devices showed high photo response from 450 to 850 nm with high EQE values, approaching 80% and the corresponding integrated current J_{cal} values are 22.14 and 20.45 mA cm^{-2}, well matched with the *J-V* test (Figure 1c). However, PBTIC-*m*-2F2T based devices showed much weaker photo response and the EQE was lower than 40%, which resulted in a significant decrease of the integrated J_{cal} of 9.53 mA cm^{-2}. The higher photo response of *γ*-position based polymers over that of the mixed polymers indicated that precise control of the molecular configuration helps to advance the J_{sc} in the devices.

In order to further understand the effect of configuration control on the charge transport properties, the space-charge-limited current (SCLC) measurements were made and the hole- and electron-only diodes with device structures of ITO/PEDOT:PSS/PBDBT-2F:acceptor/MoO_3/Ag and ITO/ZnO/PBDBT-2F: acceptor/PDINO/Al were fabricated. The corresponding hole and electron mobility curves are shown in Figure S10, Supporting Information, and the results are summarized in Table S3, Supporting Information. It was found that both hole mobility and electron mobility of the PM6: PBTIC-*γ*-2F2T blend ($\mu_h = 2.6 \times 10^{-4}$ cm^2 v^{-1} s^{-1}, $\mu_e = 1.8 \times 10^{-4}$ cm^2 v^{-1} s^{-1}) and the PM6: PBTIC-*γ*-2T blend ($\mu_h = 1.3 \times 10^{-5}$ cm^2 v^{-1} s^{-1}, $\mu_e = 5.7 \times 10^{-5}$ cm^2 v^{-1} s^{-1}) are higher than that of the PM6: PBTIC-*m*-2F2T blend ($\mu_h = 8.9 \times 10^{-5}$ cm^2 v^{-1} s^{-1}, $\mu_e = 6.4 \times 10^{-6}$ cm^2 v^{-1} s^{-1}). Further, the charge transport of the PM6: PBTIC-*γ*-2F2T blend (μ_h/μ_e = 1.4) and the PM6: PBTIC-*γ*-2T blend (μ_h/μ_e = 1.6 for PBTIC-*γ*-2T) were more balanced than that of the PM6: PBTIC-*m*-2F2T blend (μ_h/μ_e = 2.0). The better carrier transport properties of the *γ*-position based polymers are due to the improved intermolecular interactions, increased molecular planarity, and optimized morphology which helps to suppress the accumulation and recombination of charges. Accordingly, an investigation of charge recombination in the devices was performed by measurement of the change in the photocurrent with light intensity (P_{light}). The relationships between J_{sc} and P_{light} for PBTIC-*γ*-2F2T, PBTIC-*γ*-2T, and PBTIC-*m*-2F2T were used as an exponential factor to reflect the bimolecular recombination.[41] As shown in **Figure 2**a, J_{sc} and P_{light}, plotted with dual logarithmic coordinates, obtained slopes (α) of the three

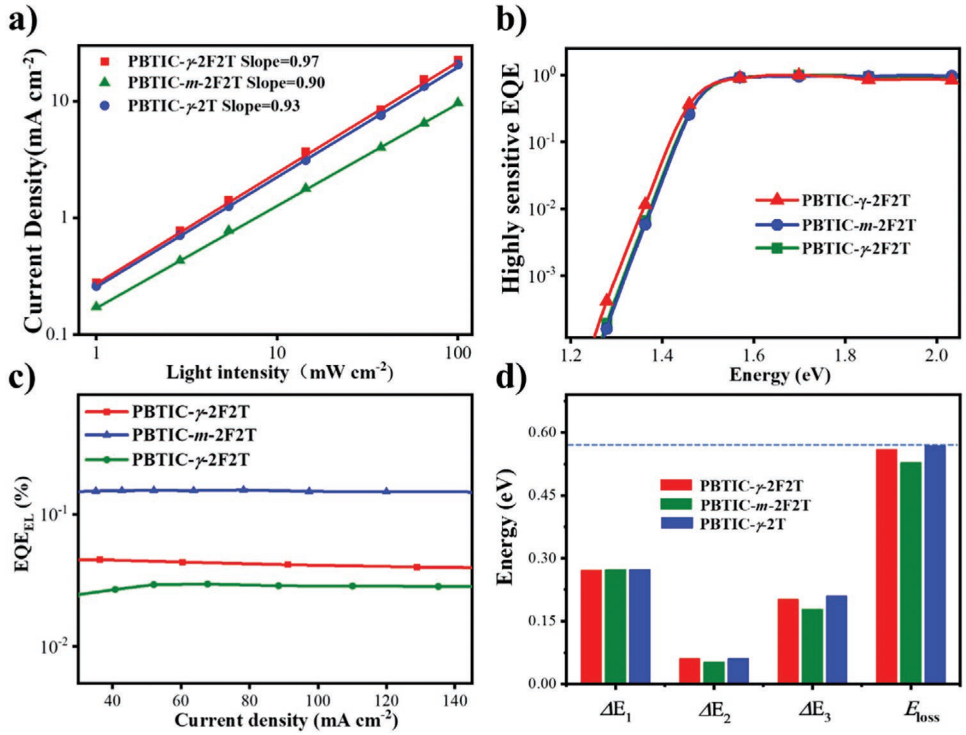

Figure 2. a) Double logarithmic plots of J_{sc} versus P_{light}. b) EL quantum efficiencies of the PBTIC-*γ*-2F2T, PBTIC-*m*-2F2T, and PBTIC-*γ*-2T based devices. c) The FTPS-EQE curves of PBTIC-*γ*-2F2T, PBTIC-*m*-2F2T, and PBTIC-*γ*-2T based devices. d) Energy loss of PBTIC-*γ*-2F2T, PBTIC-*m*-2F2T, and PBTIC-*γ*-2T based devices.

acceptor-based devices of 0.97, 0.93, and 0.90, respectively. In principle, the closer of the gradient, α to 1 means better exciton transport property and lower photocurrent loss, which enables a higher FF. Apparently, both PBTIC-γ-2F2T and PBTIC-γ-2T based device showed higher slopes (α) than that of PBTIC-*m*-2F2T, and this was consistent with their higher J_{sc} and FF.

2.4. Investigation of Voltage Loss

To achieve insight into the effects of configurational control on the voltage loss, we performed the FTPS-EQE and EQE_{EL} measurements. Based on the previous reports,[42] the total energy loss (ΔE) originated from the three sources: (1) ΔE_1, radiative recombination loss above the bandgap; (2) ΔE_2, radiative recombination loss below the bandgap; (3) non-radiative energy loss. The equation governing this is:

$$\begin{aligned}\Delta E &= E_g - qV_{oc}\\ &= \left(E_g - qV_{OC}^{SQ}\right) + \left(qV_{OC}^{SQ} - qV_{OC}^{rad}\right) + \left(qV_{OC}^{rad} - V_{oc}\right)\\ &= \Delta E_1 + \Delta E_2 + \Delta E_3\end{aligned} \tag{1}$$

E_g is the estimated bandgap based on the intersection of the maximum and the edge of the EQE spectrum of each device. The obtained bandgaps of the PBTIC-γ-2F2T, PBTIC-*m*-2F2T, PBTIC-γ-2T based devices are 1.51, 1.52, and 1.52 eV respectively (Table S4, Supporting Information). According to the Shockley–Queisser theory,[43] the three devices present a similar ΔE_1 of ≈0.272 eV. We measured ΔE_2 from the FTPS-EQE spectra of the three devices shown in Figure 2b, and the calculated values were determined to be 0.060, 0.061, and 0.052 eV, respectively. For the third part of the voltage loss, the EQE_{EL} experiments of the solar cells were carried out and the values of each device were evaluated with the equation: $\Delta E_3 = -kT\ln(EQE_{EL})$

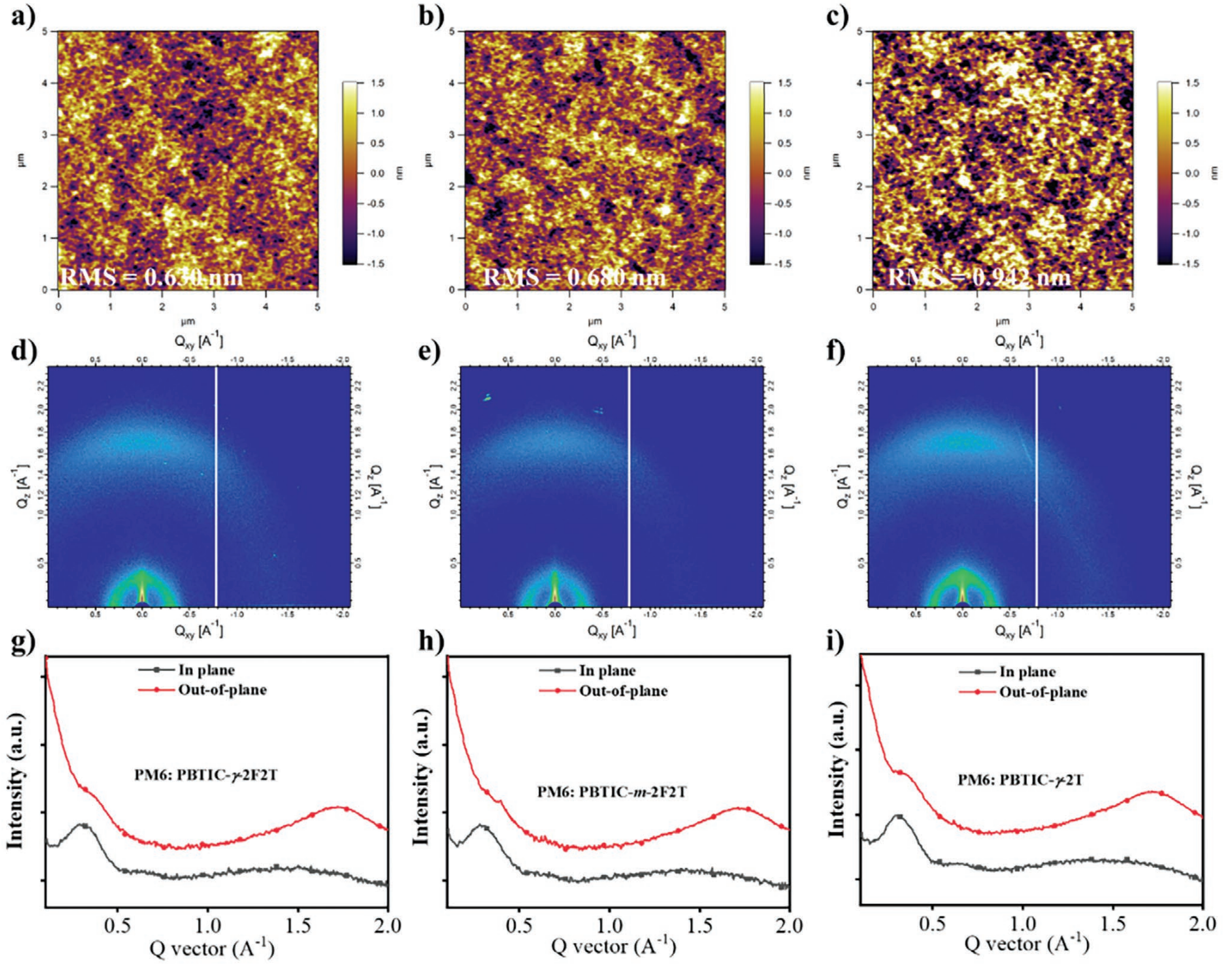

Figure 3. a–c) AFM height images of PM6:PBTIC-γ-2F2T, PM6:PBTIC-*m*-2F2T, and PM6:PBTIC-γ-2T. d–f) 2D GIWAXS patterns of PM6:PBTIC-γ-2F2T, PM6:PBTIC-*m*-2F2T ,and PM6:PBTIC-γ-2T. g–i) 1D line-cuts in the in-plane and out-of-plane directions of PM6:PBTIC-γ-2F2T, PM6:PBTIC-*m*-2F2T, and PM6:PBTIC-γ-2T.

as shown in Figure 2c. Interestingly, the PBTIC-*m*-2F2T based device showed the highest EQE_{EL} value of 9.97×10^{-4} which corresponded with the lowest ΔE_3 of 0.179 eV. This apparently low voltage loss accounts for the highest V_{oc} of the PBTIC-*m*-2F2T based solar cell. PBTIC-*γ*-2F2T based devices showed an EQE_{EL} value of 4.10×10^{-4} slightly higher than that of PBTIC-*γ*-2T (3.01×10^{-4}). The ΔE_3 was calculated to be 0.202 and 0.210 eV for the two polymer acceptors. The non-radiative energy loss (ΔE_3) of the three polymers was among the lowest values reported to date, and contribute to the lower total voltage loss (ΔE) and the higher V_{oc}.

2.5. Morphology Study of Blend Films

In order to investigate the effects of configurational control on the morphologies, atomic force microscopy (AFM) and grazing incidence wide-angle X-ray scattering (GIWAXS) were employed and the results are shown in **Figure 3**. As shown in the height images, all of the blend films exhibited a smooth surface with a root-mean-square roughness (RMS) value of no more than 1.0 nm. Among the three blend films, the PM6: PBTIC-*γ*-2F2T blend film showed a RMS value of 0.630 nm which is slightly smaller than that of PM6: PBTIC-*m*-2F2T and PM6: PBTIC-*γ*-2T whose RMS values are 0.680 and 0.942 nm. The lower RMS value means a smoother surface of the blend film, which suggests better carrier transport properties in the devices. GIWAXS was applied to measure the intermolecular packing properties and the crystallinity.[44] The 2D GIWAXS patterns and 1D line cuts of the blend films are shown in Figure 3d–i, and the corresponding parameters are summarized in Table S5, Supporting Information. It was found that PM6: PBTIC-*γ*-2F2T blend film showed a lamellar stacking peak (100) at 0.304 $Å^{-1}$ ($d_L \approx 20.67$ Å) in the q_{xy} axis direction and is similar to PM6: PBTIC-*m*-2F2T and PM6: PBTIC-*γ*-2T blend films which have peaks at 0.289 $Å^{-1}$ ($d_L \approx 21.74$ Å) and 0.306 $Å^{-1}$ ($d_L \approx 20.53$ Å), respectively. This suggests a face-on orientation for the three acceptors in the blend films. In the q_z axis direction, the lamellar packing peaks (010) of PM6: PBTIC-*γ*-2F2T and PBTIC-*γ*-2T were observed at 1.724 $Å^{-1}$ and 1.721 $Å^{-1}$ with calculated π-π stacking distances of 3.64 and 3.65 Å respectively, which were slightly smaller than the PBTIC-*m*-2F2T based blend films (1.714 $Å^{-1}$, $d_\pi \approx 3.67$ Å). The smaller π–π stacking distance implies a higher intermolecular charge transport, which is consistent with the higher mobilities obtained from the photovoltaic tests. Hence, the results obtained from the AFM and GIWAXS measurements imply that the *γ*-position based polymers blend films exhibit proper orientation, smaller π-π stacking distance, and smoother surface which is beneficial for carrier transport in the vertical direction and improves the photovoltaic performance.

3. Conclusion

In summary, we successfully separated *γ*-Br-IC and *δ*-Br-IC in gram scale and synthesized four polymer acceptors, namely PBTIC-*γ*-2F2T, PBTIC-*δ*-2F2T, PBTIC-*m*-2F2T, and PBTIC-*γ*-2T based on the strategy of configurational control of monomers. It was found that the polymerization at different sites has significant effects on the properties of the materials. The *γ*-position based polymer, PBTIC-*γ*-2F2T, has proper crystallinity and good miscibility with polymer donors, resulting in an excellent photovoltaic performance with a PCE of 14.34%. This is one of the highest values delivered by all-polymer solar cells to date. The *δ*-position based polymer, PBTIC-*δ*-2F2T exhibits strong aggregation and is almost insoluble in common solvents. This hinders subsequent studies of physicochemical, and results in almost zero (0.02%) in photovoltaic efficiency. The mix-position based polymer, PBTIC-*m*-2F2T, shows a relatively low photovoltaic performance with a PCE of 3.26%, which proves that precise control of the position for the polymerization has a significant effect on the performance of OSCs. PBTIC-*γ*-2T, obtained from the polymerization of non-fluorinated 2,2,-bithiophene and *γ*-position based monomer, also showed good performance with a high PCE, approaching 12%. These results show that the precise control of molecular configuration can enhance charge carrier mobility, decrease π–π stacking distance, and thus afford a promising strategy for providing high performance all-polymer solar cells.

Supporting Information

Supporting Information is available from the Wiley Online Library or from the author.

Acknowledgements

H.W. and H.C. contributed equally to this work. This work was financially supported by the National Natural Science Foundation of China (51773087, 21733005, 21975115, and 51903116), Shenzhen Fundamental Research Program (JCYJ20170817111214740, JCYJ20180302180238419, KQJSCX20180319114442157), Guangdong Provincial Key Laboratory of Catalysis (2020B121201002), Guangdong Innovative and Entrepreneurial Research Team Program (2016ZT06G587) and Shenzhen Sci-Tech Fund (KYTDPT20181011104007). The authors also thank the SUSTech Core Research Facilities for the AFM and TEM measurements.

Conflict of Interest

The authors declare no conflict of interest.

Data Availability Statement

Research data are not shared.

Keywords

all-polymer solar cells, bromination, configurational isomers, polymer acceptors, polymerization

Received: January 26, 2021
Revised: March 24, 2021

[1] G. Yu, A. J. Heeger, *J. Appl. Phys.* **1995**, *78*, 4510.
[2] G. Yu, J. Gao, J. C. Hummelen, F. Wudl, A. J. Heeger, *Science* **1995**, *270*, 1789.
[3] C. Lee, S. Lee, G. U. Kim, W. Lee, B. J. Kim, *Chem. Rev.* **2019**, *119*, 8028.
[4] Z. Genene, W. Mammo, E. Wang, M. R. Andersson, *Adv. Mater.* **2019**, *31*, 1807275.
[5] Z. G. Zhang, Y. Li, *Angew. Chem., Int. Ed.* **2020**, *60*, 4422.
[6] F. Peng, K. An, W. Zhong, Z. Li, L. Ying, N. Li, Z. Huang, C. Zhu, B. Fan, F. Huang, Y. Cao, *ACS Energy Lett.* **2020**, *5*, 3702.
[7] W. Wang, Q. Wu, R. Sun, J. Guo, Y. Wu, M. Shi, W. Yang, H. Li, J. Min, *Joule* **2020**, *4*, 1070.
[8] T. Jia, J. Zhang, W. Zhong, Y. Liang, K. Zhang, S. Dong, L. Ying, F. Liu, X. Wang, F. Huang, Y. Cao, *Nano Energy* **2020**, *72*, 104718.
[9] H. Sun, H. Yu, Y. Shi, J. Yu, Z. Peng, X. Zhang, B. Liu, J. Wang, R. Singh, J. Lee, Y. Li, Z. Wei, Q. Liao, Z. Kan, L. Ye, H. Yan, F. Gao, X. Guo, *Adv. Mater.* **2020**, *32*, 2004183.
[10] Q. Fan, Q. An, Y. Lin, Y. Xia, Q. Li, M. Zhang, W. Su, W. Peng, C. Zhang, F. Liu, L. Hou, W. Zhu, D. Yu, M. Xiao, E. Moons, F. Zhang, T. D. Anthopoulos, O. Inganäs, E. Wang, *Energy Environ. Sci.* **2020**, *13*, 5017.
[11] X. Zhan, Z. a. Tan, B. Domercq, Z. An, X. Zhang, S. Barlow, Y. Li, D. Zhu, B. Kippelen, S. R. Marder, *J. Am. Chem. Soc.* **2007**, *129*, 7246.
[12] J. Yang, B. Xiao, A. Tang, J. Li, X. Wang, E. Zhou, *Adv. Mater.* **2019**, *31*, 1804699.
[13] G. Wang, F. S. Melkonyan, A. Facchetti, T. J. Marks, *Angew. Chem., Int. Ed.* **2019**, *58*, 4129.
[14] H. You, D. Kim, H.-H. Cho, C. Lee, S. Chong, N. Y. Ahn, M. Seo, J. Kim, F. S. Kim, B. J. Kim, *Adv. Funct. Mater.* **2018**, *28*, 1803613.
[15] J. Qu, Z. Mu, H. Lai, M. Xie, L. Liu, W. Lu, W. Chen, F. He, *ACS Appl. Energy Mater.* **2018**, *1*, 833.
[16] Y. Zhao, H. Wang, S. Xia, F. Zhou, Z. Luo, J. Luo, F. He, C. Yang, *Chem. Eur. J.* **2018**, *24*, 4149.
[17] H. Yan, Z. Chen, Y. Zheng, C. Newman, J. R. Quinn, F. Dötz, M. Kastler, A. Facchetti, *Nature* **2009**, *457*, 679.
[18] R. Stalder, J. Mei, J. Subbiah, C. Grand, L. A. Estrada, F. So, J. R. Reynolds, *Macromolecules* **2011**, *44*, 6303.
[19] X. Long, Z. Ding, C. Dou, J. Zhang, J. Liu, L. Wang, *Adv. Mater.* **2016**, *28*, 6504.
[20] K. Feng, J. Huang, X. Zhang, Z. Wu, S. Shi, L. Thomsen, Y. Tian, H. Y. Woo, C. R. McNeill, X. Guo, *Adv. Mater.* **2020**, *32*, 2001476.
[21] Z. G. Zhang, Y. Yang, J. Yao, L. Xue, S. Chen, X. Li, W. Morrison, C. Yang, Y. Li, *Angew. Chem., Int. Ed.* **2017**, *56*, 13503.
[22] H. Yao, F. Bai, H. Hu, L. Arunagiri, J. Zhang, Y. Chen, H. Yu, S. Chen, T. Liu, J. Y. L. Lai, Y. Zou, H. Ade, H. Yan, *ACS Energy Lett.* **2019**, *4*, 417.
[23] Y. Meng, J. Wu, X. Guo, W. Su, L. Zhu, J. Fang, Z. G. Zhang, F. Liu, M. Zhang, T. P. Russell, Y. Li, *Sci. China: Chem.* **2019**, *62*, 845.
[24] Y. Li, Z. Jia, Q. Zhang, Z. Wu, H. Qin, J. Yang, S. Wen, H. Y. Woo, W. Ma, R. Yang, J. Yuan, *ACS Appl. Mater. Interfaces* **2020**, *12*, 33028.
[25] Q. Fan, W. Su, S. Chen, W. Kim, X. Chen, B. Lee, T. Liu, U. A. Méndez-Romero, R. Ma, T. Yang, W. Zhuang, Y. Li, Y. Li, T. S. Kim, L. Hou, C. Yang, H. Yan, D. Yu, E. Wang, *Joule* **2020**, *4*, 658.
[26] Q. Fan, W. Su, S. Chen, T. Liu, W. Zhuang, R. Ma, X. Wen, Z. Yin, Z. Luo, X. Guo, L. Hou, K. Moth-Poulsen, Y. Li, Z. Zhang, C. Yang, D. Yu, H. Yan, M. Zhang, E. Wang, *Angew. Chem.* **2020**, *59*, 19835.
[27] Q. Fan, R. Ma, T. Liu, W. Su, W. Peng, M. Zhang, Z. Wang, X. Wen, Z. Cong, Z. Luo, L. Hou, F. Liu, W. Zhu, D. Yu, H. Yan, E. Wang, *Sol. RRL* **2020**, *4*, 2000142.
[28] J. Wu, Y. Meng, X. Guo, L. Zhu, F. Liu, M. Zhang, *J. Mater. Chem. A* **2019**, *7*, 16190.
[29] H. Yao, L. K. Ma, H. Yu, J. Yu, P. C. Y. Chow, W. Xue, X. Zou, Y. Chen, J. Liang, L. Arunagiri, F. Gao, H. Sun, G. Zhang, W. Ma, H. Yan, *Adv. Energy Mater.* **2020**, *10*, 2001408.
[30] J. Du, K. Hu, L. Meng, I. Angunawela, J. Zhang, S. Qin, A. Liebman-Pelaez, C. Zhu, Z. Zhang, H. Ade, Y. Li, *Angew. Chem., Int. Ed.* **2020**, *59*, 15181.
[31] J. W. Lee, C. Sun, B. S. Ma, H. J. Kim, C. Wang, J. M. Ryu, C. Lim, T.-S. Kim, Y.-H. Kim, S. K. Kwon, B. J. Kim, *Adv. Energy Mater.* **2021**, *11*, 2003367.
[32] H. Wang, L. Han, J. Zhou, T. Liu, D. Mo, H. Chen, H. Lai, N. Zheng, Z. Xie, W. Zheng, F. He, *CCS Chem.* **2020**, *2*, 2591.
[33] J. Qu, D. Li, H. Wang, J. Zhou, N. Zheng, H. Lai, T. Liu, Z. Xie, F. He, *Chem. Mater.* **2019**, *31*, 8044.
[34] Z. Luo, T. Liu, R. Ma, Y. Xiao, L. Zhan, G. Zhang, H. Sun, F. Ni, G. Chai, J. Wang, C. Zhong, Y. Zou, X. Guo, X. Lu, H. Chen, H. Yan, C. Yang, *Adv. Mater* **2020**, *32*, 2005942.
[35] H. Lai, H. Chen, J. Zhou, P. Chao, T. Liu, X. Chang, N. Zheng, Z. Xie, F. He, *Iscience* **2019**, *17*, 302.
[36] J. W. Jo, J. W. Jung, H. Ahn, M. J. Ko, A. K. Y. Jen, H. J. Son, *Adv. Energy Mater.* **2017**, *7*, 1601365.
[37] Q. Zhao, J. Qu, F. He, *Adv. Sci.* **2020**, *7*, 2000509.
[38] Q. Zhang, M. A. Kelly, N. Bauer, W. You, *Acc. Chem. Res.* **2017**, *50*, 2401.
[39] H. Lai, Q. Zhao, Z. Chen, H. Chen, P. Chao, Y. Zhu, Y. Lang, N. Zhen, D. Mo, Y. Zhang, F. He, *Joule* **2020**, *4*, 688.
[40] H. Lai, F. He, *Adv. Energy Mater.* **2020**, *10*, 2070190.
[41] S. R. Cowan, A. Roy, A. J. Heeger, *Phys. Rev. B* **2010**, *82*, 245207.
[42] J. Liu, S. Chen, D. Qian, B. Gautam, G. Yang, J. Zhao, J. Bergqvist, F. Zhang, W. Ma, H. Ade, O. Inganäs, K. Gundogdu, F. Gao, H. Yan, *Nat. Energy* **2016**, *1*, 16089.
[43] W. Shockley, H. J. Queisser, *J. Appl. Phys.* **1961**, *32*, 510.
[44] J. Mai, Y. Xiao, G. Zhou, J. Wang, J. Zhu, N. Zhao, X. Zhan, X. Lu, *Adv. Mater.* **2018**, *30*, 1802888.